The total wind load can be calculated by

$$P_a(t) = \mu_s A \rho_a V_a^2(t)/2 \tag{10}$$

where $V_a(t)$ is the total wind speed and ρ_a represents the air density (1.235 kg/m^3). The drag coefficients of transmission tower are determined based on the standard (DL/T5154-2012 2012).

4. CASE STUDY

4.1 FEM of transmission tower-line system

A real operational transmission line is employed, with the exposure category of type B. The transmission conductor and ground wire types are LGJX-240/30 and GJX-50, respectively. The insulator string is FC70P/146, with a total length of 1.8 m and a mass of 26.46 kg. The ANSYS software is used to build the finite element model (FEM) of the transmission tower-line system, as shown in Fig. 1. The BEAM188 element is used to simulate the tower member, and the transmission line and insulator string are modeled via the LINK180 element.

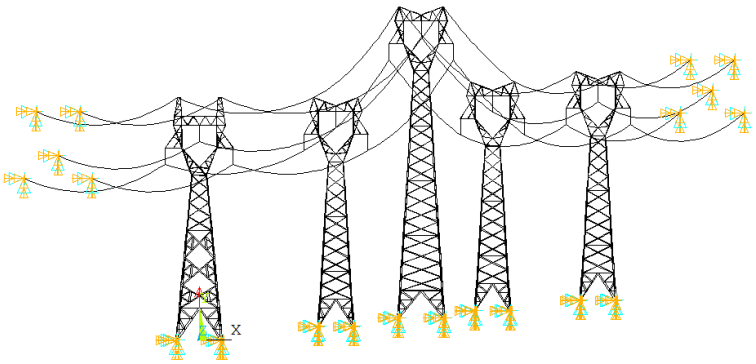

Fig. 1 FEM of the transmission tower-line system

4.2 Field measurements during super typhoon Mangkhut

A structural health monitoring (SHM) system was installed on tower #32, as shown in Fig. 2. Sixteen strain sensors and three accelerometers are mounted to measure the tower response, and an ultrasonic anemometer is used to measure the wind speed and direction. To eliminate the shielding effect of tower itself on the anemometer, a special support was designed to keep the anemometer as far away from the tower as possible.

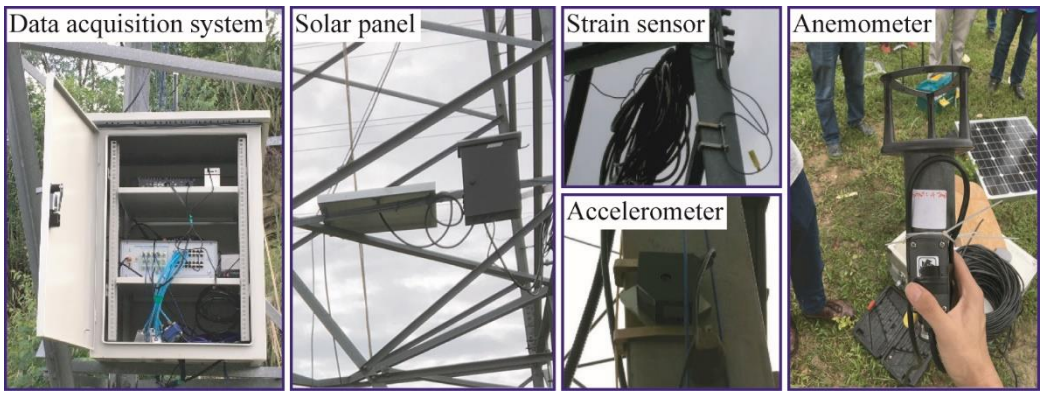

Fig. 2 Structural health monitoring system of tower #32

The dynamic responses of tower #32 under the super typhoon Mangkhut were recorded. The wind speed and direction of typhoon Mangkhut are plotted in Fig. 3. The transmission line direction is 29° north by east, and the wind direction at 0 degrees denotes north and increases clockwise. During the Mangkhut making landfall, the maximum gust wind speed reached 42 m/s, and the wind speed gradually decreased to 0 at approximately 1700 UTC on 16 September. The wind direction was stable at 35° north by west at first, and then the wind speed changed sharply, being stable at 30° south by east. The wind direction changed approximately 180°, indicating that the typhoon eye passed over tower #32 during this period.

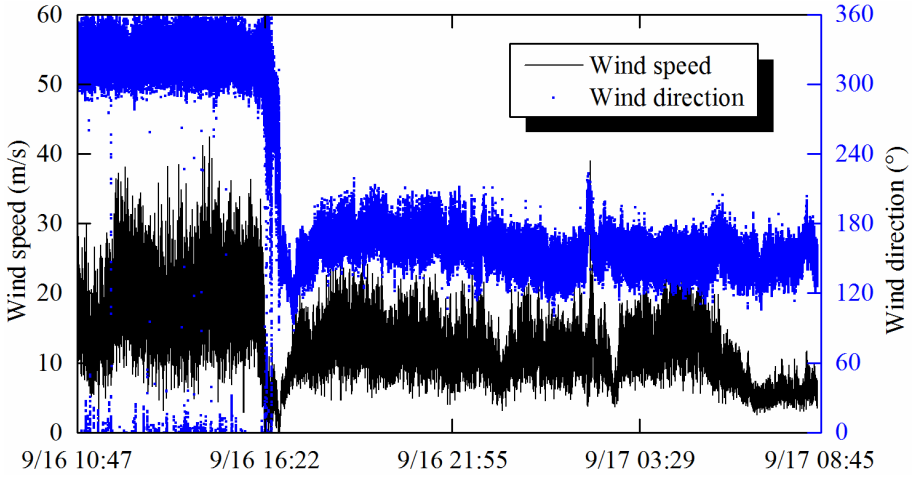

Fig. 3 Time history curves of the wind speed and wind direction of typhoon Mangkhut

At approximately 1700 UTC on 16 September, the wind direction changes dramatically, and the corresponding data are eliminated to reduce the errors due to stationary assumption. All of the measured data are divided into 10 min for each group, and then the GRFs are calculated based on Eq. (4), as shown in Fig. 4. At low wind speeds, the influence of the wind speed on the GRF is inapparent; at high wind speeds,

greater than 10 m/s, the larger wind speeds lead to greater GRFs. The influence of the turbulence intensity on the GRF is very obvious with a higher turbulence intensity leading to a greater GRF. In addition, the GRFs in different tower positions are different, and a higher position results in a larger GRF. Given the Chinese standard (DL/T5154-2012 2012), the GRF of this tower should be 1.29, which is smaller than the measured results.

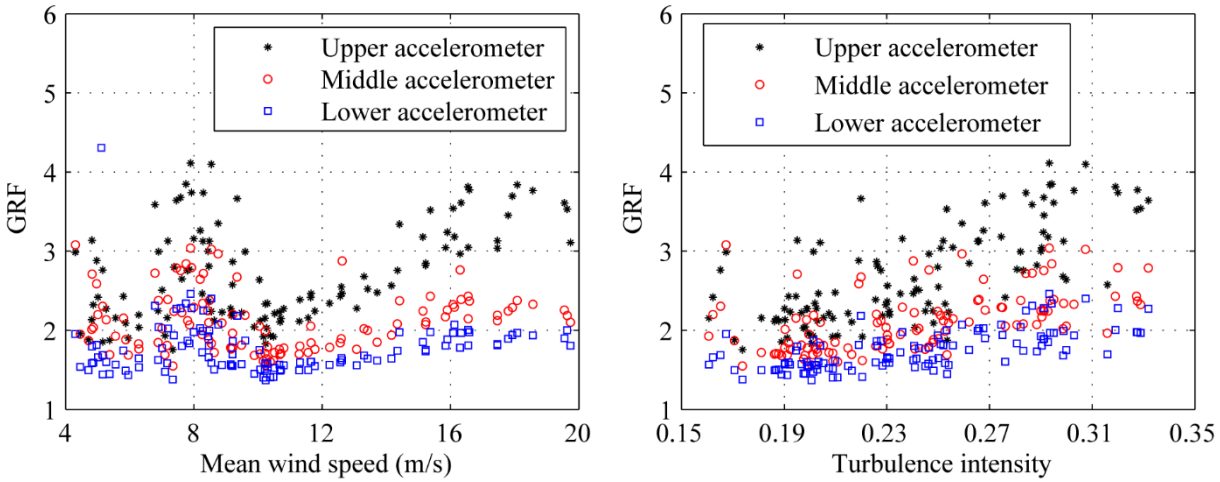

(a) Influence of the mean wind speed (b) Influence of the turbulence intensity

Fig. 4 GRFs in the transverse direction calculated based on the field-measured data

4.3 Numerical validation

In the field measurements, the wind speed and wind direction are uncontrollable, and only the measured data can be analyzed, which has many limitations. Thereby, the analysis of many other conditions that have not been measured depends greatly on the numerical simulation. In this subsection, the GRFs of tower #32 are calculated based on the numerical simulation, which is then validated by comparing with Fig. 4, providing the basis for the parametric analysis in the next section.

The basic wind speed is 15 m/s, and the fluctuating wind speeds are generated via both the Davenport and Shiyuan spectra. By applying the wind loads on the FEM, the dynamic response is then calculated. Fig. 5 displays the time history curves of the tip displacement for tower #32 under both synoptic and typhoon winds. The mean displacements are very similar, while the RMS of displacement under the typhoon is larger than that under the synoptic winds, indicating that the GRFs under the typhoon must be greater.

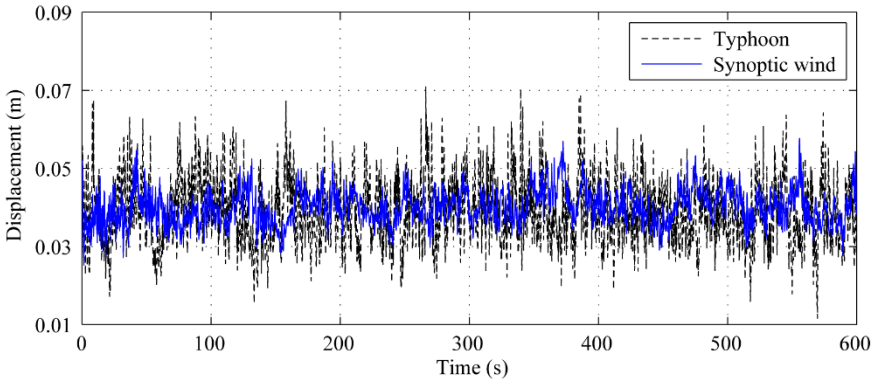

Fig. 5 Tower tip displacements of tower #32 under typhoon and synoptic wind

The simulated turbulence intensities of the typhoon and synoptic wind are 0.1796 and 0.1074, respectively, and are located at the lower level of the measured results. To better reflect the GRFs at the similar turbulence intensity level of numerical simulation, the measured GRFs with the two smallest turbulence intensities (17.38% and 16.06%) are selected for comparison with the simulation results. Fig. 6 shows the comparison of the GRFs between the numerical simulation and field measurements. The Chinese standard recommends that the GRF takes 1.29 for this employed tower, which is much smaller than both the simulated and measured results, indicating that the Chinese standard underestimates the gust response effect of the employed transmission tower. Meanwhile, the GRFs under the typhoon are larger than those under the synoptic wind, and the main reason is that the turbulence intensity of typhoon is larger. In addition, the simulated GRFs under the typhoon are located among the field measurement results for the higher altitudes, demonstrating that using the numerical method to estimate GRFs is feasible.

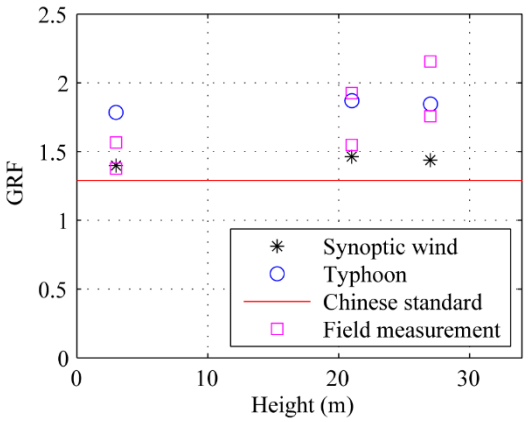

Fig. 6 Comparison of GRFs between the numerical simulation and field measurements

5. SUMMARY AND CONCLUSIONS

In this paper, the measured GRFs under the super typhoon Mangkhut were obtained according to the SHM system installed on tower #32. Then, the FEM of transmission tower-line system was established to simulate the dynamic response to further calculate the GRFs, which was then validated by being compared with the field measurements. The conclusions drawn from the whole paper are summarized below:

1) The GRFs under the typhoon are larger than those under the synoptic wind, and the main reason is that the turbulence intensity of typhoon is greater.
2) The recommended GRF in the Chinese standard is much smaller than both the simulated and measured results, indicating that the Chinese standard underestimates the gust response effect on a transmission tower, which needs to be further improved.

Acknowledgments

This research was supported by the National Natural Science Foundation of China (grant no. 51708089).

REFERENCES

Aboshosha, H., Elawady, A., El Ansary, A., El Damatty, A. (2016), "Review on dynamic and quasi-static buffeting response of transmission lines under synoptic and non-synoptic winds", *Engineering Structures*, **112**, 23-46.

ASCE-No.74 2010. Guidelines for Electrical Transmission Line Structural Loading. ASCE, USA.

Chen, X., Kareem, A. (2004), "Equivalent static wind loads on buildings: New model", *Journal of Structural Engineering*, **130** (10), 1425-1435.

Davenport, A.G. (1961), "The spectrum of horizontal gustiness near the ground in high winds", *Journal of the Royal Meteorological Society*, **87** (372), 194-211.

Davenport, A.G., Sparling, B.F. (1992), "Dynamic gust response factors for guyed towers", *Journal of Wind Engineering & Industrial Aerodynamics*, **41-44**, 2237-2248.

DL/T5154-2012 2012. Technical code for the design of tower and pole structures of overhead transmission line. China Planning Press, Beijing.

Fu, X., Li, H.-N., Yi, T.-H. (2015), "Research on motion of wind-driven rain and rain load

acting on transmission tower", *Journal of Wind Engineering and Industrial Aerodynamics*, **139**, 27-36.

Harikrishna, P., Shanmugasundaram, J., Gomathinayagam, S., Lakshmanan, N. (1999), "Analytical and experimental studies on the gust response of a 52 m tall steel lattice tower under wind loading", *Computers & Structures*, **70**, 149-160.

Hua, X.G., Chen, Z.Q., Yang, J.B., Niu, H.W., Chen, B. (2014), "Turbulence integral scale corrections to experimental results of aeroelastic models with large geometric scales: Application to gust loading factor of a transmission line tower", *Advances in Structural Engineering*, **17** (8), 1189-1197.

Kareem, A., Zhou, Y. (2003), "Gust loading factor—past, present and future", *Journal of Wind Engineering & Industrial Aerodynamics*, **91**, 1301-1328.

Shinozuka, M., Jan, C.-M. (1972), "Digital simulation of random processes and its applications", *Journal of Sound and Vibration*, **25** (1), 111-128.

Simiu, E. (1976), "Equivalent static wind loads for tall building design", *Journal of the Structural Division*, **102** (4), 719-737.

Vellozzi, J., Cohen, E. (1968), "Gust response factors", *Journal of the Structural Division*, **94** (ST6), 1295-1313.

Vickery, B.J. 1970. On the reliability of gust loading factors, in: Proceedings of the Technical Meeting Concerning Wind Loads on Buildings and Structures, 93-104. National Bureau of Standards.

Xie, Q., Cai, Y., Xue, S. (2017), "Wind-induced vibration of UHV transmission tower line system: Wind tunnel test on aero-elastic model", *Journal of Wind Engineering & Industrial Aerodynamics*, **171**, 219-229.

Zhang, Z.-Q., Li, H.-N., Li, G., Wang, W.-M., Tian, L. (2013), "The numerical analysis of transmission tower-line system wind-induced collapsed performance", *Mathematical Problems in Engineering*, **2013**, Article ID 413275.